

2016

A morphometric analysis of ultrastructural dynamics in the murine glomerulus following surgically-induced renal hypertension

<https://hdl.handle.net/2144/17039>

Boston University

BOSTON UNIVERSITY
SCHOOL OF MEDICINE

Thesis

**A MORPHOMETRIC ANALYSIS OF ULTRASTRUCTURAL DYNAMICS IN
THE MURINE GLOMERULUS FOLLOWING SURGICALLY-INDUCED
RENAL HYPERTENSION**

by

JAMES WARE STEVENSON

B.S., Providence College, 2014

Submitted in partial fulfillment of the
requirements for the degree of
Master of Science

2016

© 2016 by
JAMES WARE STEVENSON
All rights reserved

Approved by

First Reader

Joel Henderson, M.D., Ph.D.
Assistant Professor of Pathology & Laboratory Medicine

Second Reader

Mostafa Belghasem, M.D., Ph.D.
Post-Doctoral Associate, Pathology & Laboratory Medicine

ACKNOWLEDGMENTS

I would like to thank Doctors Joel Henderson, Mostafa Belghasem, and Philip Bondzie for providing training, materials, and direction throughout this project. I would also like to acknowledge the hospitality of the Department of Anatomic Pathology at Boston Medical Center and Dr. Hui Chen of the electron microscopy facility, without whom this work would not have been possible. Finally, thank you to F.S. O'Brien and J.R. Hooper for their support and assistance.

**A MORPHOMETRIC ANALYSIS OF ULTRASTRUCTURAL DYNAMICS IN
THE MURINE GLOMERULUS FOLLOWING SURGICALLY-INDUCED
RENAL HYPERTENSION**

JAMES WARE STEVENSON

ABSTRACT

Chronic kidney disease (CKD) and end stage renal disease (ESRD) are significant causes of adult morbidity and mortality worldwide. Though these conditions are common, the mechanisms of pathogenesis in kidney disease are poorly understood. Genetic predisposition has been established in the African American population; however this does not explain the ubiquity of CKD in the United States and abroad. Diabetes and hypertension are the two most frequently occurring co-morbidities in kidney disease and both have been identified as putative sources of injury to the delicate filtering structures of the kidney. Furthermore, the intrinsic functional relationship between the cardiovascular and renal organ systems adds to the plausibility of a hemodynamic cause. In light of this knowledge, we aim to explore the roles of genetic predisposition and hypertension in the pathogenesis and progression of CKD.

The filtering apparatus of the kidney, the glomerulus, is a looping tuft of capillaries specialized to allow the passage of water and certain substances from the blood while restricting others. Glomeruli at the corticomedullary boundary of the kidney experience blood pressures closer to those in systemic arterioles and are subject to similar

hemodynamic stresses. To evaluate the role of hypertension in CKD, we employed a well-known model of hypertensive kidney disease in mice involving uninephrectomy (UNX), subcutaneous implantation of a timed-release pellet containing the active aldosterone precursor deoxycorticosterone acetate (DOCA), and a high-salt diet. Given the role of heritability in human CKD pathogenesis, we applied the DOCA-UNX model in two strains of mice with differing susceptibility to kidney damage, the 129S6 and C57BL/6 strains, to evaluate the effects of genetic predisposition. Mice were subjected to varying lengths of hypertension exposure and their kidneys were subsequently examined by transmission electron microscopy (TEM). Ultrastructural lesions of glomeruli were evaluated by a renal pathologist and assigned subjective pathology scores based on the extent and severity of involvement.

We hypothesized that certain glomerular lesions, particularly those involving the podocytes of the visceral epithelium, would increase in severity in mice with heritable susceptibility (129S6) as well as those with longer exposure to glomerular hypertension. Our observations demonstrate these hypotheses are partially correct. By TEM histopathology, mouse strain was found to have a significant effect on the severity of certain epithelial lesions while duration of hypertension had a significant effect on the overall morphological pathology of the podocytes, glomerular basement membrane, and glomerulus as a whole. These results provide a promising foundation for further investigation of the pathogenesis of CKD in mice.

TABLE OF CONTENTS

| | |
|--------------------------------------|-----|
| ACKNOWLEDGMENTS | iv |
| ABSTRACT..... | v |
| TABLE OF CONTENTS..... | vii |
| LIST OF TABLES | ix |
| LIST OF FIGURES | x |
| LIST OF ABBREVIATIONS..... | xi |
| INTRODUCTION | 1 |
| EPIDEMIOLOGY | 1 |
| GLOMERULAR PHYSIOLOGY | 3 |
| GFR, ALBUMINURIA, & STAGING..... | 6 |
| PATHOPHYSIOLOGY OF CKD | 9 |
| PATHOGENESIS OF CKD | 12 |
| DIAGNOSTIC ELECTRON MICROSCOPY | 15 |
| METHODS | 17 |
| INDUCTION OF HYPERTENSION | 17 |
| TISSUE PROCESSING..... | 17 |
| SECTIONING & STAINING..... | 18 |
| ELECTRON MICROSCOPY & IMAGING..... | 20 |

| | |
|----------------------------|----|
| HISTOPATHOLOGY | 20 |
| STATISTICAL ANALYSIS | 21 |
| RESULTS | 22 |
| DISCUSSION | 31 |
| REFERENCES | 41 |
| CURRICULUM VITAE..... | 46 |

LIST OF TABLES

| <u>Table</u> | <u>Title</u> | <u>Page</u> |
|--------------|--|-------------|
| 1 | CKD staging and prognostic criteria | 8 |
| 2 | p-values from 2-way ANOVA of histopathology scores | 24 |
| 3 | Results of post-hoc tests | 26 |

LIST OF FIGURES

| <u>Figure</u> | <u>Title</u> | <u>Page</u> |
|---------------|---|-------------|
| 1 | The glomerular filtration barrier | 4 |
| 2 | Foot process effacement | 11 |
| 3 | Mean histopathology scores with significant strain and exposure effects | 25 |
| 4 | Mean histopathology scores in post-hoc tests | 27 |
| 5 | Representative images of foot process effacement | 28 |
| 6 | Representative images of podocyte vacuoles and microvillous change | 29 |
| 7 | Representative images of capillary loops from controls and animals in all experimental groups | 30 |
| 8 | Membrane-bound structures in Bowman's space | 39 |
| 9 | Epithelial lysis and denudation of the glomerular basement membrane | 40 |

LIST OF ABBREVIATIONS

| | |
|----------------|------------------------------------|
| ACR | Albumin:creatinine ratio |
| BL/6 | C57BL/6 |
| BS..... | Bowman's space |
| CKD | Chronic kidney disease |
| DOCA | Deoxycorticosterone acetate |
| DOCA-UNX | DOCA/Uninephrectomy model |
| ECF | Extracellular fluid |
| ESRD | End stage renal disease |
| FP | Foot process |
| FPE..... | Foot process effacement |
| FSGS..... | Focal segmental glomerulosclerosis |
| GBM | Glomerular basement membrane |
| GFR..... | Glomerular filtration rate |
| GHT | Glomerular hypertension |
| MCD | Minimal-Change Disease |
| TEM | Transmission electron microscopy |
| UNX..... | Uninephrectomy |

INTRODUCTION

Chronic kidney disease (CKD) and end-stage renal disease (ESRD) are common causes of adult morbidity and mortality which threaten the well-being of individuals and place a significant burden on the healthcare economy as a whole. Affecting over 1 in 10 adults in worldwide²³, CKD encompasses a range of chronic conditions disrupting the vital filtration processes of the kidneys, resulting in persistent physiologic and metabolic disturbances. When renal function becomes insufficient to meet physiological demands CKD reaches its natural conclusion, a terminal stage known as ESRD or “kidney failure”, necessitating either dialysis or transplantation for survival. Both terminal interventions and long-term management options for CKD are costly and as a result, kidney disease at all stages accounts for a significant portion of healthcare spending in the United States. In 2013, CKD alone consumed one-fifth of Medicare spending for patients over 65 while life-preserving measures for ESRD patients constituted 7% of overall Medicare spending⁵⁵. Indeed, the steep human and monetary costs of CKD merit thorough investigation of its character.

EPIDEMIOLOGY

CKD affects approximately 15% of adults in the United States and half of those aged 70 years or older^{7,55}. In 2013, the United States Renal Data System reported that ESRD, defined as patients with very high-risk CKD, affected over 660,000 Americans with an overall mortality rate of 138 per 1,000 patients. Of greater concern, less than 50% of

individuals with stage 3 or 4 CKD are aware of their disease, jeopardizing opportunities to prevent it from progressing further^{7,55}.

It is well-established that African Americans are at increased risk of developing ESRD^{28,29,53}, contributing further to the adversity of a vulnerable and socioeconomically disadvantaged population. Indeed, low socioeconomic status has also been associated with CKD^{6,56}, compromising a significant proportion of this population. African Americans in 2013 were three times more likely to develop ESRD and experienced a prevalence 3.7 times higher than caucasians⁵⁵. This increased risk is partially attributable to genetic predisposition^{18,54} as well as a greater prevalence of medical risk factors including diabetes and cardiovascular disease^{16,26}. Furthermore, data suggest that African Americans with these risk factors are not sufficiently aware of their CKD risk, stymying efforts for early and coordinated intervention^{16,26}.

While prevalent in the United States, CKD and ESRD are also familiar problems around the world, with estimates placing the global prevalence of CKD over 10%²³. According to data regarding disease-specific treatment measures, namely dialysis and renal transplantation, the global incidence of treated ESRD is highly variable. The greatest incidence of ESRD is found in Southeast Asia, Japan, and North America, while much of Europe and Russia show the lowest⁵⁵. It should be noted that available data is limited mainly to developed countries due to challenges in both diagnosis and reporting, excluding Africa and most of Central Asia. Causality for CKD internationally is also difficult to measure, however it is noted that some logical causes, such as infectious disease and

environmental exposures, are generally more common in developing nations than developed ones^{23,38}.

GLOMERULAR PHYSIOLOGY

In the kidney, filtration of the extracellular fluid (ECF) is accomplished at the glomerulus—a biological sieve that allows the passage of certain plasma components into a specialized series of tubules which monitor and adjust their content before excretion in the urine. The glomerulus, encapsulated within a renal corpuscle, comprises a looping tuft of capillaries lined by a specialized interdigitating epithelium and structurally supported by a cell/matrix composite termed the mesangium. Material filtered from the capillary blood must travel through a 3-part barrier, each component of which contributes to the selectivity of the molecular sieve (**Figure 1**). Once through the filtration barrier, the “ultrafiltrate” composed primarily of water, salts, and small molecules enters the extracellular Bowman’s space (BS) within the corpuscle before draining to the renal tubule system.

The first layer of the glomerular filtration barrier is a fenestrated endothelium with perforations up to 100 nm in diameter, allowing free passage of water and other molecules into the glomerular basement membrane (GBM) composed largely of type IV collagen, laminins, glycosaminoglycans, and other anionic substances^{25,42}. Beyond the GBM the lining epithelium is formed by podocytes—highly specialized cells which embrace the structures of the glomerulus and anchor themselves to the basement membrane with characteristic foot processes (FPs). Interdigitating FPs from neighboring podocytes jointly sheath the capillary loops, limiting the area for filtration to narrow (20-30 nm)³ filtration

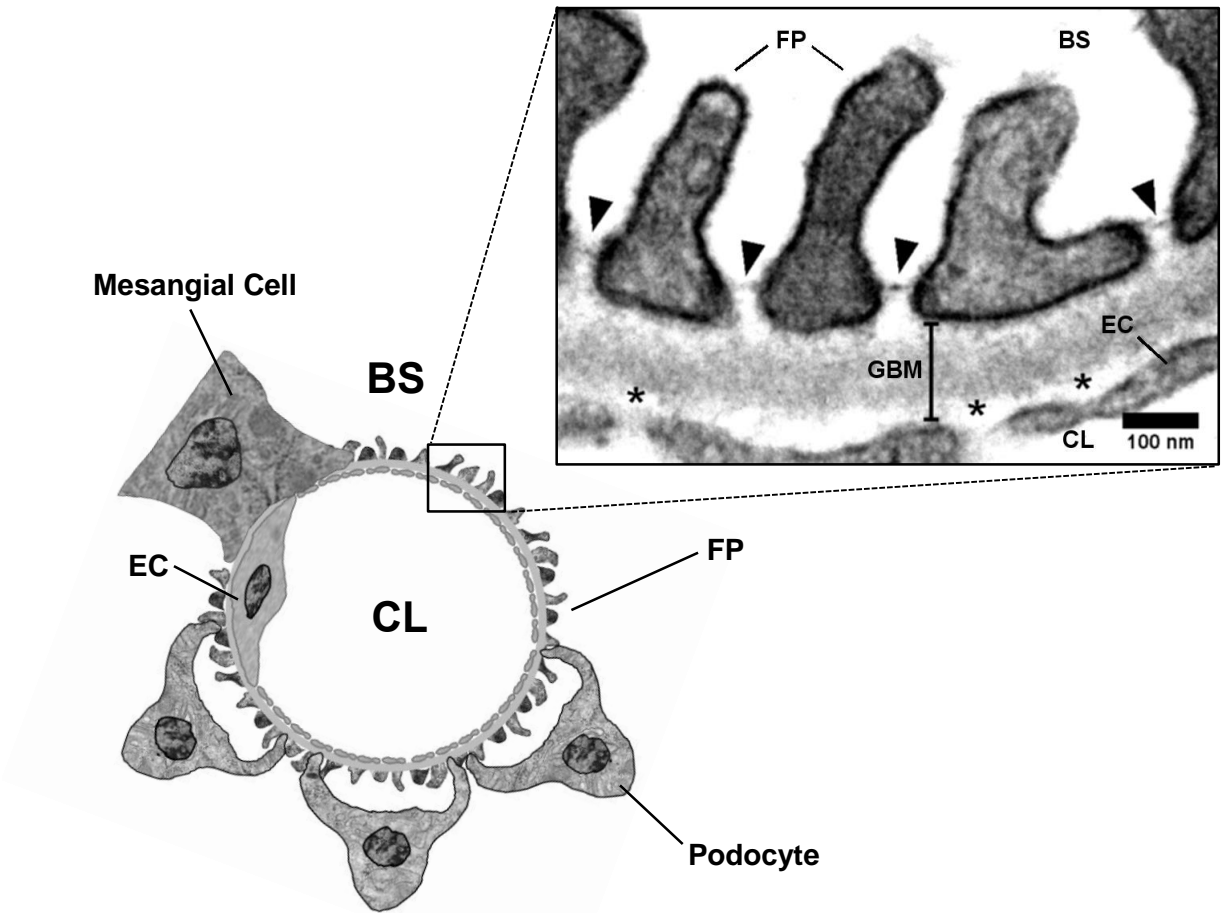


Figure 1: The glomerular filtration barrier. Capillary loops are structurally supported by mesangial cells and lined by an epithelium composed of podocytes. Ultrafiltrate passes from the blood in the capillary lumen (CL) to the Bowman's Space (BS) first through endothelial cells (EC) perforated by fenestrations up to 100 nm in diameter (asterisks). After crossing the glomerular basement membrane (GBM, barred line), the ultrafiltrate must then pass through a slit diaphragm (arrowheads) spanning the filtration slit between interdigitating foot processes (FP). The glycoprotein coat of foot processes can be observed as a fuzzy outline. Illustration by Mostafa Belghasem, reproduced and adapted by permission. Pictured (inlay): Digital transmission electron micrograph of normal 129S6 mouse kidney, taken at 50,000X magnification. Tissue prepared as described in methods. Image taken by author and labelled using ImageJ⁴⁸.

slits between adjacent processes. At the filtration slit, adjoining FPs are anchored to the membrane by adhesion proteins and bridged primarily by interacting domains of the protein nephrin, forming a specialized slit diaphragm⁴² which participates in the filtration process.

The ultrastructural and molecular composition of the filtration barrier is specialized to restrict the permeability of specific substances based on their size and charge. Endothelial fenestrations are of sufficient caliber to allow the passage of water and some substances while preventing large macromolecules and cells from exiting the capillary lumen. In the GBM, interwoven matrix proteins form another physical barrier excluding molecules with a molecular radius approximately that of serum albumin (36 Å) or larger^{4,42}. Additionally, anionic glycoproteins and glycosaminoglycans within the GBM create an electrostatic barrier that repels negatively charged molecules including several plasma proteins^{4,25,46}. Molecules that permeate the GBM are then subject to additional electrostatic and physical hindrance at the filtration slit and within Bowman's space, as anionic proteins within the narrow slit diaphragm and a negatively-charged glycoprotein coat surrounding foot processes further repel large anionic molecules^{42,49}.

While it is widely acknowledged that the GBM is the primary mediator of permeability in the glomerulus, podocytes and endothelial cells contribute to the constitution of the GBM as well as the overall permeability of the barrier. In development, both endothelial cells and podocytes synthesize basement membrane proteins^{1,51}, and expression of GBM-binding adhesion proteins in podocytes is necessary for the construction of an effective filtration barrier¹³. The remarkably stable structure of the GBM

allows the respective epithelial cells to decrease production of its components after development, however their continued presence is necessary to ensure its stability¹.

GFR, ALBUMINURIA, & STAGING

Because of the kidney's essential function as a hemodynamic regulator, the interactions between the cardiovascular and renal organ systems must be understood to properly assess kidney function both qualitatively and quantitatively. Filtration across the glomerular barrier is driven by Starling forces, owing to the supra-venous hydraulic pressures experienced within the glomerulus and the near absence of oncotic pressure in the Bowman's space of a normally functioning renal corpuscle³. The volume of plasma filtered into Bowman's space per unit time, referred to as the glomerular filtration rate (GFR), can therefore be calculated as a function of these forces. GFR is proportional to the difference in hydraulic pressures between the capillary lumen and BS (net hydraulic force) minus the difference in oncotic pressures between compartments (net oncotic force)³.

GFR is considered the best quantitative indicator of overall kidney function and has served this role for decades^{36,39,43}. The renal clearance of creatinine, an endogenous component of blood plasma that is freely filtered from the glomerulus and not reabsorbed by the renal tubules, can be used to generate an estimate of GFR^{36,37,41}. Because CKD is most generally defined as a progressive deterioration of the filtering capacity of the kidneys, GFR is a critical factor in the diagnosis and staging of the disease. Early criteria for clinical identification and monitoring therefore defined CKD as having a GFR < 60 mL/min/1.73 m², with a GFR < 15 mL/min/1.73 m² indicating ESRD⁴³.

In addition to reduced GFR, the definition of CKD includes an indication of ongoing kidney damage (≥ 3 months) as determined by the presence of pathological abnormalities on biopsy or constitutional abnormalities in the urine^{39,43}. A practical indicator of glomerular injury is the presence of protein, specifically serum albumin, in the urine, as a normally functioning filtration barrier should prevent most albumin from entering the ultrafiltrate. Albuminuria is measured clinically as the ratio of albumin to creatinine concentration in the urine (albumin:creatinine ratio—ACR), with an ACR ≥ 300 mg/g indicating overt clinical albuminuria^{39,43}.

Staging of CKD originated with simple GFR-based criteria outlined in a 2002 report of the Kidney Disease Outcomes Quality Initiative and was later revised in 2011 to improve coherence with patient outcomes^{39,40}. The most recent guidelines from the Kidney Disease: Improving Global Outcomes commission therefore include a two-part staging system, taking both GFR and albuminuria into account and emphasizing prognostic factors by associating stages with relative mortality risk categories (**Table 1**)³⁹. Individuals in the moderate, high, or very high risk categories are considered to have overt CKD, and from 2007-2012 the prevalence of U.S. adults in each risk category was 9.8%, 2.3%, and 1.7%, respectively⁵⁵.

Table 1: Chronic kidney disease staging and prognostic criteria. Albuminuria measured as urine albumin:creatinine ratio in mg/g. GFR ranges presented in mL/min per 1.73 m² body surface area. Colors indicate adjusted relative risk of mortality due to kidney disease. Green indicates no/minimal risk, yellow indicates mild risk, orange indicates moderate risk, and red indicates severe/imminent risk. CKD is defined as a GFR < 60 mL/min per 1.73 m² for at least 3 months. Nephrotic syndrome defined as albuminuria >2000 mg/g ACR. Adapted from Levey et al., 2011.

| | | | Albuminuria Stages | | | | |
|--------------------------|------------------------------|--------|--------------------------------------|--------|---------------------|------------------------------------|-------|
| | | | A1 (optimal to acceptable) | | A2 (high) | A3 (very high to nephrotic) | |
| | | | <10 | 10-29 | 30-299 | 300-1999 | >2000 |
| <u>GFR Stages</u> | G1 (high to optimal) | >105 | Green | Green | Yellow | Orange | Red |
| | | 90-104 | Green | Green | Yellow | Orange | Red |
| | G2 (mild) | 75-89 | Green | Green | Yellow | Orange | Red |
| | | 60-74 | Green | Green | Yellow | Orange | Red |
| | G3a (mild-moderate) | 45-59 | Yellow | Yellow | Orange | Red | Red |
| | G3b (moderate-severe) | 30-44 | Orange | Orange | Red | Red | Red |
| | G4 (severe) | 15-29 | Red | Red | Red | Red | Red |
| | G5 (ESRD) | <15 | Red | Red | Red | Red | Red |

PATHOPHYSIOLOGY OF CKD

CKD is characterized by an accumulation of pathological abnormalities and functional deficiencies caused by chronic injury to the delicate microstructures of the kidney, resulting in the progressive deterioration of ECF regulation. Patients with CKD and ESRD therefore experience severe physiologic and metabolic disturbances, such as uremia and nephrosis, which precipitate death if left untreated³⁴. Glomerular injury begins at the ultrastructural level, where physiologic insults abolish permselectivity by disrupting and disorganizing the structure of the filtration barrier. Podocytes in particular exhibit well-documented adaptive changes in the context of cellular injury which have been observed in a range of pathologies associated with CKD, including the nephrotic syndrome and focal segmental glomerulosclerosis (FSGS)^{9,15,27,34}. Indeed, evidence suggests that podocyte adaptation and injury is central to the pathophysiology of CKD.

The nephrotic syndrome, characterized by massive proteinuria (≥ 3.5 g/day or ≥ 2000 ACR), hypoalbuminemia, and generalized edema^{34,39}, is a direct result of declining kidney function in the late stages of CKD and has been associated with morphological changes in podocytes since the 1950's¹⁵. Podocytes in the kidneys of nephrotic patients exhibit a distinct pattern of FP retraction referred to as foot process effacement (FPE), resulting in widened FPs spanning broader distances of the GBM and reducing the frequency of filtration slits^{9,34,49} (**Figure 2**). Furthermore, varying degrees of FPE are associated with specific glomerular disease states¹⁰, however it remains unclear whether FPE is a cause or consequence of glomerular injury. Evidence from animal models suggests that effacement can precede proteinuria in some cases⁴⁹, but conflicting data from clinical

studies find a lack of association between the degree of effacement and level of proteinuria in multiple glomerulopathies². Nevertheless, FPE continues to be a consistent finding in the histology of patients with proteinuria and is certainly relevant to the pathophysiology of CKD.

Podocyte stress and injury manifest at the light microscopic scale in the form of FSGS, a condition in which some, but not all glomeruli exhibit sclerotic lesions in isolated segments of the capillary tuft^{9,34}. A model for the pathogenesis of FSGS hinges on the terminally differentiated nature of podocytes, which renders them unable to replace themselves in the event that cell stress reaches a critical maximum^{9,49}. It is suggested that these critically injured podocytes lose their attachments to the GBM and eventually detach from the glomerulus, leaving a segment that is inevitably repaired by matrix deposition and scar formation^{9,33}. As a result, sclerosed segments accumulate until function is so impeded that the glomerulus as a whole ceases to operate. This theory is supported by the observations that podocyte density at the glomerulus is lower in individuals with kidney disease⁵⁷, viable and non-viable podocytes are excreted in the urine at a higher rate in CKD patients^{57,58}, and the rate of podocyturia can be used as a specific marker of ongoing kidney damage⁵⁸.

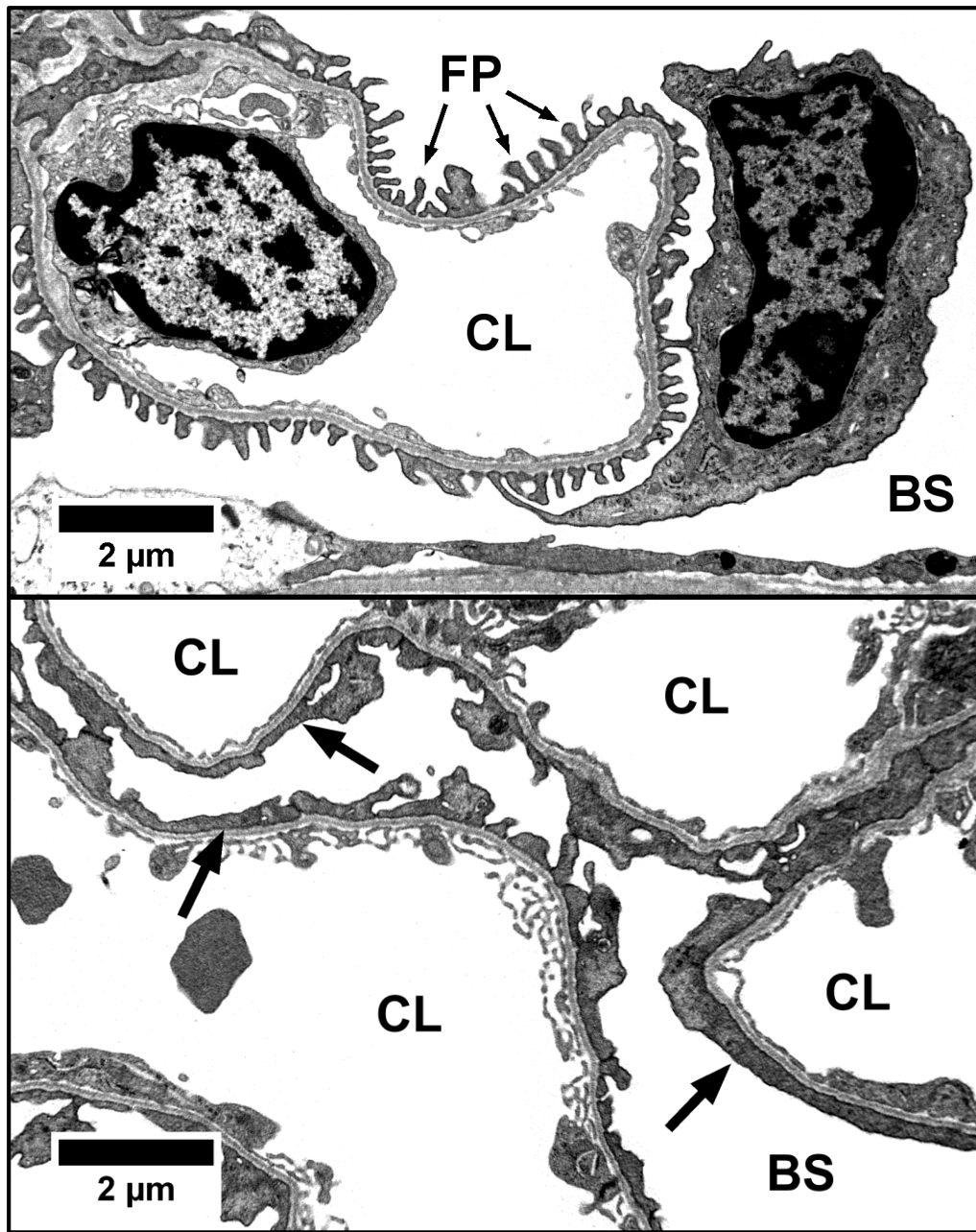


Figure 2: Foot process effacement. Effacement of FPs is a characteristic finding in the glomerular ultrastructure of patients with CKD-associated conditions, including nephrosis and FSGS. Pictured: Digital transmission electron micrographs of 129S6 mouse kidney with normal podocyte architecture (top) and prominent FPE (bottom). Effaced foot processes are labeled with arrows in the bottom image. Both images taken at 10,000X magnification and processed using ImageJ⁴⁸. Tissue prepared as described in methods. BS= Bowman's space, CL= Capillary lumen, FP= Foot process.

Structural and functional changes in CKD-associated pathologies are not limited to the podocyte. Changes in the thickness and composition of the GBM are frequently reported in the renal histology of nephrotic patients as well as the presence of deposits and additional matrix material in sclerotic segments of the glomerulus^{9,19,31,34}. Progression from epithelial damage to sclerosis also involves expansion of the mesangium, with an increase in the density of both mesangial cells and matrix in the glomerulus^{19,30,31}. Finally, swelling of the endothelium has been observed in experimental models of FSGS as well as other renal and cardiovascular disorders²⁴. Despite the range of structures affected in glomerulopathy, the podocyte ties together several of these pathological abnormalities, given its role in maintaining the GBM, protecting the capillary loop from sclerosis, and regulating endothelial cell function^{1,24,31}.

PATHOGENESIS OF CKD

Conceptual models of CKD suggest that its development is a result of ongoing tissue injury followed by processes of repair and adaptation that may themselves contribute to disease^{39,40}. Lesions found in the kidneys of CKD patients commonly resemble hypertensive nephrosclerosis and diabetic glomerulosclerosis, both of which are products of hemodynamic disorders³⁸. Moreover, hypertension and diabetes are the most frequently occurring co-morbidities in CKD patients, suggesting that extra-renal hemodynamic pathologies predispose and perpetuate kidney damage^{52,55}. Studies of risk factors confirm that these conditions increase susceptibility to CKD which strengthens the argument for hemodynamic etiologies^{8,21,44,52}, however causal relationships between extra-renal disease

and CKD are somewhat obscure. The current study explores the role of hypertension in CKD pathogenesis.

Systemic hypertension causes measurable increases in the intra-capillary pressures of juxtamedullary glomeruli, a condition known as glomerular hypertension (GHT)¹⁴. The association of cardiovascular disorders with renal pathology draws upon the success of GHT animal models in precipitating glomerular injury^{14,30} as well as the observation that sclerotic lesions of the glomerulus are strikingly similar to those seen in atherosclerosis¹¹. In order to assess the role of GHT in glomerulopathy, an examination of hemodynamic forces in hypertension and the mechanical properties of the glomerulus is necessary.

The hydraulic pressure gradient that drives filtration at the glomerulus does so at the cost of subjecting the capillary wall and associated structures to considerable physical forces. In the context of GHT these forces increase in magnitude, intensifying circumferential stress and tension in the capillary wall¹⁴. The turgor of the GBM therefore provides a critical line of defense against capillary distension, but the elastic properties of this membrane have not yet been quantified and the GBM alone seems incapable of negotiating such wall tension^{30,32}. It has been suggested that podocytes may counteract distending forces via cytoskeletal contraction mechanisms, yet the contractile forces of podocytes have also not been thoroughly studied and the notion that foot processes are capable of transmitting those forces is questionable^{14,32}. In fact, experiments subjecting rat glomeruli to high perfusion pressures demonstrate that the glomerulus fails to mitigate drastic increases in wall tension, resulting in capillary distension with an increase in GBM

area over 50%³². Augmented transmural hydraulic force is therefore a putative source of injury in CKD, prompting further investigation of the role of GHT in pathogenesis.

Animal models have proved indispensable for the study of kidney disease in hypertension. One such model simulates the physiologic disturbances present in systemic hypertension to examine the consequences of acquired GHT^{12,14}. In this model, rats or mice are subjected to uninephrectomy (UNX), administration of an exogenous form of the active aldosterone precursor deoxycorticosterone acetate (DOCA), and increased NaCl intake, representing a multi-hit approach that involves both loss of functional renal mass and ECF volume retention¹². Animals subjected to this treatment have been observed to exhibit histologic and physiologic features of progressive kidney injury, including glomerulosclerosis, glomerular capillary distension, FPE, podocyte loss, mesangial expansion, and marked albuminuria^{12,30}. In sum, the DOCA/uninephrectomy model (DOCA-UNX) of GHT is an effective tool for simulating and assessing the effects of hypertension on kidney function. Our study employs the DOCA-UNX method to induce GHT and examine its effects on renal histopathology in mice.

In light of evidence that genetic factors may contribute to CKD^{17,18,54}, we also set out to determine if heritable susceptibility in mice influences renal histopathology in the context of GHT. Towards this end, we examined the histopathological effects of GHT in two different strains of mice, the 129S6 and C57BL/6 strains. These strains have been shown to respond to renal insults differently, with the 129S6 strain considered susceptible to kidney damage while the C57BL/6 strain is considered resistant^{5,47}. Additionally, experiments with renal ablation techniques have demonstrated that genetic factors in 129S6

mice are associated with a greater degree of overall histopathology, blood pressure increase, and albuminuria compared to C57BL/6 mice⁴⁷, however data on the severity of specific lesions is lacking. The current study aims to address this deficiency by examining the severity of CKD-associated lesions in both strains.

DIAGNOSTIC ELECTRON MICROSCOPY

Transmission electron microscopy (TEM), which allows specimen observation at magnifications in excess of 100,000X, has been used for the purpose of renal biopsy for many years and its contribution to efficient diagnosis is invaluable^{35,50}. The intricate ultrastructure of the kidney necessitates the use of TEM to identify lesions undetectable by light microscopy. An important example of the need for TEM in renal pathology is the case of Minimal-Change Disease (MCD). In MCD, glomeruli appear normal by light microscopy despite a clinical presentation of severe nephrosis during childhood³⁴. Closer examination by TEM reveals pronounced effacement of FPs, a lesion too small to observe in light microscopy. This lesion is considered to be the source of proteinuria in these patients³⁴. While the cause of podocyte injury in MCD is not yet known, TEM is essential for its diagnosis.

In addition to FPE, lesions commonly observed by TEM in renal biopsy include thickening or thinning of the GBM, the presence of protein and immune deposits, and newly synthesized GBM beneath injured endothelial cells (double contours), all of which are implicated in a variety of renal diseases^{19,34,35}. This study employs TEM to identify and characterize the severity of these specific glomerular lesions in hypertensive mice. Lesions

considered are listed in **Table 2** and represent all four structural domains of the glomerulus: Visceral epithelium (podocytes), GBM, endothelium, and mesangium.

Studies using the remnant kidney model to examine kidney injury in C57BL/6 and 129S6 mice have shown differing physiological responses but have not thoroughly explored the ultrastructure of these animals⁴⁷. Given the close interrelation of structure and function in the kidney, such information may be useful in directing future studies to identify molecular mechanisms involved in CKD pathogenesis. We hypothesize that those morphological changes observed in the kidneys of human CKD patients should be present also in the kidneys of mice and would be observed to a higher degree in the injury-prone 129S6 mice. Furthermore, those changes most closely associated with the physiological hallmarks of CKD, decreased GFR and pronounced albuminuria, are suspected to be severe in susceptible mice with increasing exposure to GHT—changes such as FPE, FP irregularity, and GBM thickness variations. We aim to subjectively quantify these ultrastructural dynamics in order to shed light on the pathogenesis of CKD in hypertensive mice with differing susceptibilities to kidney disease. Towards this end, we have performed a morphometric analysis of glomerular histopathology by TEM in 129S6 and C57BL/6 mice subjected to the DOCA-UNX procedure and describe our results here.

METHODS

INDUCTION OF HYPERTENSION

At 11-13 weeks of age, male 129S6/ScEv (Taconic Biosciences) and C57BL/6 (abbreviated henceforth as BL/6) mice (Jackson Laboratory) underwent left uninephrectomy and subcutaneous implantation of a 60-day timed-release pellet containing 150 mg of deoxycorticosterone acetate (Innovative Research of America, Sarasota, FL) between the scapulae. Following surgery, mice were fed 1% NaCl solution and standard feed until euthanized at 24 hours, 7 days, or 42 days. Time zero controls were euthanized immediately following surgery. To confirm a sustained increase in blood pressure in experimental subjects, systolic blood pressure was measured via the tail cuff method (BP-2000, Visitech Systems) with measurements taken a minimum of 3 times per week until dispatch. Mice were trained for a minimum of 3 days to reduce stress associated with blood pressure measurements and the procedure was conducted in a quiet room to further maintain a normal environment.

TISSUE PROCESSING

The remaining kidney was harvested immediately after euthanasia and cut into 1 mm³ thick sections perpendicular to the long axis of the organ followed by additional radial cuts into wedge-shaped pieces to maintain orientation of tissue architecture. Dissected kidney tissue was fixed in 3% glutaraldehyde solution and stored at 4°C overnight or until further processing. Preserved tissue was rinsed in 0.1 M sodium cacodylate buffer for 10

minutes before post-fixation in 1% osmium tetroxide/0.15 M sodium cacodylate solution for one hour. The tissue was then washed in deionized water for 5 minutes and dehydrated by 5 minute treatments in a graded acetone series of 50%, 90%, 100%, 100%, and 100% solution.

For embedding in epoxy resin, osmium-fixed dehydrated tissue was first treated with a 1:1 solution of unpolymerized resin and acetone for 1 hour, then 100% resin for approximately 4 hours. Treatments in unpolymerized resin were carried out in scintillation vials on a rotating platform to ensure effective infiltration. Finally, the tissue was placed in the cap of a BEEM® capsule containing 100% epoxy resin and left overnight at 60°C. Capsules also contained a small paper identifying label at the end opposite the tissue. Resulting blocks contained flat-embedded tissue in polymerized epoxy resin.

SECTIONING & STAINING

Blocks of resin-embedded tissue were liberated from the capsule and excess resin was trimmed away from the specimen using a stainless steel razorblade. To locate areas of interest within the specimen, semi-thin 2 µm sections were cut using a fresh glass knife at a tilt angle of 3° on a Leica EM UC7 Ultramicrotome (Leica Microsystems, Buffalo Grove, IL), then floated on a droplet of water on a charged glass slide. After applying heat to remove water, sections adhered to the slide were stained with toluidine blue dye for approximately 30 seconds on heat, then rinsed with water and dabbed gently with a paper towel to remove excess stain. Stained semi-thin sections were then examined by light

microscopy to locate areas of the tissue specimen containing juxtamedullary glomeruli with patent capillary loops and minimal overt pathology.

Once a satisfactory region of tissue was located, more excess resin was trimmed away from the specimen using a stainless steel razorblade to isolate the area of interest. Next, the tissue block was cut into ultra-thin 72 nm sections using a 4 mm 45° diamond knife (Diatome, Hatfield, PA) at a tilt angle of 6° on the same ultratome used for light microscopy. To remove imperfections caused by semi-thin sectioning, 1-3 200 nm sections were cut from the surface of the specimen using the diamond knife prior to ultra-thin sectioning. Ultra-thin sections were then treated with xylene vapor to prevent wrinkling by hovering a wooden applicator saturated in liquid xylene over the sections for 3-5 seconds as they floated in the knife reservoir. Sections of satisfactory thickness and quality were then placed on heat-treated copper grids and dried on #42 filter paper in a petri dish. Ultra-thin sections were not directly manipulated in the knife reservoir before being placed on the grid.

Prior to electron microscopy, the prepared sections were stained with 4% aqueous uranyl acetate by floating grids section side-down on individual droplets of solution in a petri dish for 5 minutes at 60°C. Sections were then washed by dipping grids 50 times in and out of a large ceramic bowl containing deionized water. Next, sections were stained with 0.4% aqueous lead citrate by immersing the grid section side-up in a droplet of solution for 45 seconds at room temperature, then given a final wash in water using the dip technique described above.

ELECTRON MICROSCOPY & IMAGING

After drying on #42 filter paper, grids containing intact, stained sections were examined using a JEOL JEM-1011 transmission electron microscope (JEOL, Japan) at an accelerating voltage of 80 kV. Images were taken using a Gatan Erlangshen ES1000W side-mounted digital camera with Gatan Digital Micrograph© software (Gatan, Pleasanton, CA). Care was taken to limit imaging to juxtamedullary glomeruli with patent capillary loops and minimal overt pathology as identified via light microscopy. A minimum of 3 glomeruli were imaged in each animal at standard magnifications of 3000X, 6000X, and 10,000X for morphometric analysis. Images used for publication processed with ImageJ⁴⁸.

HISTOPATHOLOGY

A total of 24 animals were considered in this study, 12 of each strain, with each strain group comprising 3 animals per time point and 3 animals as time zero controls. Image sets from each animal were examined by an experienced renal pathologist who was blind to the experimental conditions of the animal in each set. Severity scores based on degree of involvement were assigned to various known pathological abnormalities on a subjective scale of 0-4, with 0 indicating no presence, 1 indicating isolated presence, 2 indicating mild presence (< 25% involvement), 3 indicating moderate presence (25-75% involvement), and 4 indicating severe presence (> 75% involvement). Novel abnormalities or findings were noted on a case-by-case basis but not scored for severity. All image sets contained a minimum of 50 total images at 3000X, 6000X, and 10,000X magnifications. Images

containing torn sections, obstructive artefacts, or heavy staining precipitates were excluded from the study.

STATISTICAL ANALYSIS

2-way ANOVA ($\alpha=0.05$) was performed on subjective histopathology measures followed by post-hoc Tukey multiple comparisons tests for significance. Unpaired t-tests ($\alpha=0.05$) were performed for measures of FPE and microvillous change, as described below. All statistical analysis performed using GraphPad PRISM software (GraphPad Software Inc., La Jolla, CA).

RESULTS

Image sets from 24 mice were evaluated and assigned subjective severity scores for 14 known pathological abnormalities in the 4 glomerular domains: Visceral epithelium (podocytes), basement membrane, endothelium, and mesangium. Of the 14 lesions considered, all but one (subepithelial deposits) were observed to some degree. Scores were assigned on the basis of severity, with a score of 0 indicating the lesion was not present, 1 indicating the lesion was present in an isolated region, 2 indicating < 25% involvement, 3 indicating 25-75% involvement, and 4 indicating > 75% involvement. None of the lesions we observed were of sufficient severity to merit a score of 4 during the course of the study.

2-way ANOVA reveals that significant differences were observed both between strain groups and time of exposure groups (**Table 2**). Interestingly, strain differences were observed to have an influence on the severity of specific lesions, whereas time of exposure had a greater effect on cumulative domain and overall pathology scores (**Figure 3**). We observed no significant interaction between strain and exposure effects for any of the lesions considered or cumulative scores (data not shown). Representative images of animals from all groups are shown in **Figure 7**.

Strain differences were observed exclusively within the podocyte domain (**Figure 3A-C**), which was of particular interest in this study. To further quantify differences in means between strain groups, unpaired t-tests ($\alpha=0.05$) ignoring exposure groups were performed for lesions with significant differences as determined by 2-way ANOVA (**Table 3**). We observed significant differences in the degree of FPE between the two strains of

mice ($p < 0.03$) (**Figure 3A**), with the 129S6 strain having a mean score 0.500 points greater than the BL/6 strain ($p < 0.04$) (**Figure 4A**). Other findings associated with podocyte injury, specifically cellular vacuolization ($p < 0.05$) and microvillous change ($p < 0.02$), were unexpectedly observed to a higher degree in the supposedly disease-resistant BL/6 strain (**Figure 3B, C**). Large vacuoles were observed exclusively in the podocytes of BL/6 mice (**Figure 3B**). Podocyte microvilli were observed to a higher degree in BL/6 mice, with a mean score 0.583 points greater than that of the 129S6 mice ($p < 0.02$) (**Figure 4A**). It should be noted that both microvilli and vacuoles were found in control mice, possibly pointing to a pattern of normal morphology that differs from that of humans.

Significant differences between exposure groups were observed for cumulative podocyte ($p < 0.05$), GBM ($p < 0.03$), overall pathology scores ($p < 0.03$) (**Table 2, Figure 3D-F**). As expected, these scores were all significantly higher after 42 days of exposure than at earlier time points (**Table 3**). Ignoring strain effects, mean cumulative podocyte pathology score was 1.83 points higher after 42 days of GHT than 7 days ($p < 0.05$) (**Figure 4B**). Both cumulative GBM ($p < 0.03$) and overall pathology ($p < 0.03$) scores were greater at 42 days than 1 day, with differences in means of 2.17 and 8.50, respectively (**Figure 4C, D**).

All lesions considered were observed to some degree except for subepithelial deposits. Representative images of specific lesions are shown in **Figure 5** and **Figure 6**. The most extensive FPE was observed in the 42-day exposure group of 129S6 mice (**Figure 5**), which also had a notable amount of irregularities in the GBM, mostly in the form of wide variations in thickness. BL/6 mice showed a significantly greater degree of

vacuolization and microvillous degeneration compared to the 129S6 strain (**Figure 6**), both of which are considered pathological lesions in humans. Remarkably, these lesions are well-represented within both time zero and 1-day exposure groups (**Figure 3B, C**).

Table 2: p-values from 2-way ANOVA of histopathology scores. 2-way ANOVA ($\alpha=0.05$) was performed to identify significant differences in histopathology scores between strain groups and exposure groups as well as interaction effects. Significant effects ($p < 0.05$) are indicated with an asterisk (*). Mouse strain had a significant effect on FP effacement, vacuolization, and microvillous change, while time of exposure had a significant effect on cumulative podocyte, GBM, and overall scores. No significant interaction effects between strain and exposure were observed (data not shown). Subepithelial deposits were not found in any specimen. Statistics performed using GraphPad Prism software.

| Domain | Pathology | Time of Exposure | Mouse Strain |
|-------------------------|-------------------------|------------------|----------------|
| Podocytes | FP Effacement | 0.155 | 0.0262* |
| | FP Irregularity | 0.130 | 0.332 |
| | Vacuolization | 0.181 | 0.0499* |
| | Microvillous Change | 0.163 | 0.0114* |
| | Subepithelial Deposits | N/A | N/A |
| | Cumulative | 0.0422* | 0.834 |
| GBM | Thinning | 0.0777 | 0.434 |
| | Irregularity | 0.255 | 0.0702 |
| | Cumulative | 0.0212* | 0.350 |
| Endothelium | Swelling | 0.357 | 0.317 |
| | Double Contours | 0.310 | 0.115 |
| | Subendothelial Deposits | 0.585 | >0.999 |
| | Cumulative | 0.235 | 0.189 |
| Mesangium | Swelling | 0.137 | 0.490 |
| | Matrix Expansion | 0.0725 | 0.644 |
| | Cellular Expansion | 0.137 | 0.490 |
| | Deposits | 0.379 | 0.165 |
| | Cumulative | 0.0785 | 0.335 |
| Cumulative Score | | 0.0289* | 0.964 |

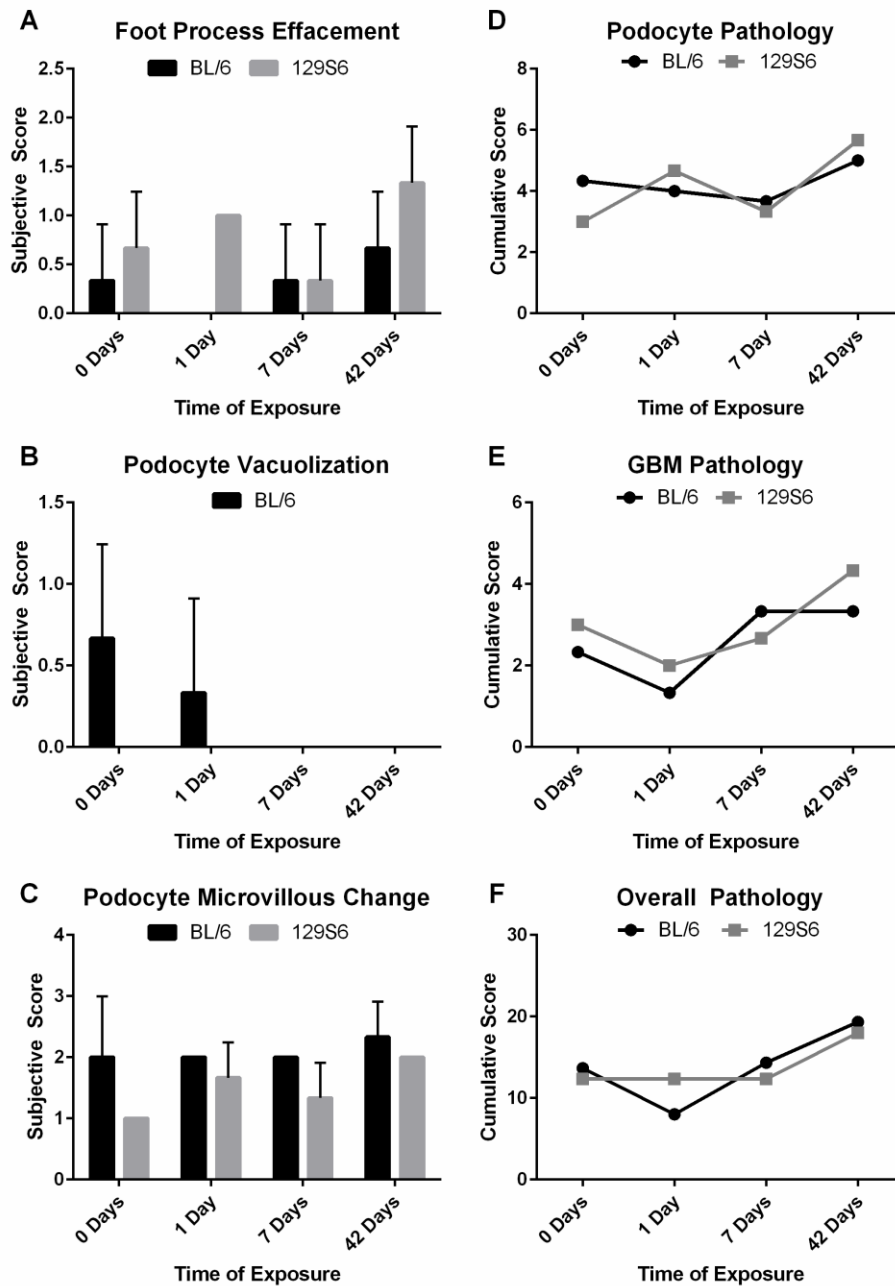


Figure 3: Mean histopathology scores with significant strain and exposure effects. Left column (A-C): Mouse strain was observed to have a significant effect on FPE ($p=0.262$) (A), podocyte vacuolization ($p=0.0499$) (B), and microvillous change ($p=0.0114$) (C). Error bars represent standard deviations. Right column (D-F): Time of exposure was observed to have a significant effect on cumulative podocyte ($p=0.0422$) (D), GBM ($p=0.0212$) (E), and overall pathology scores ($p=0.0289$) (F). Graphs of means and standard deviations derived from 2-way ANOVA analysis, performed and generated using GraphPad Prism software.

Table 3: Results of post-hoc tests. Top: Results of unpaired t-tests ($\alpha=0.05$) for FPE, podocyte vacuolization, and microvillous change scores. Differences in means ($\Delta\mu$) presented \pm standard deviation (SD). p-values from 2-way ANOVA ($p_{(ANOVA)}$) and t-tests ($p_{(t-test)}$) shown in first and last columns, respectively. FPE was more severe in the 129S6 strain, while microvillous change was more severe in the BL/6 strain. Podocyte vacuolization was only observed in the BL/6 strain. Bottom: Results (p-values) of 2-way ANOVA for cumulative podocyte, GBM, and overall pathology scores as well as significant results from post-hoc Tukey tests. Cumulative podocyte scores were significantly greater at day 42 than day 7, whereas cumulative GBM and overall pathology scores were significantly greater at day 42 than day 1. Significant effects ($p < 0.05$) are indicated with an asterisk (*). All statistics performed using GraphPad Prism software.

| Strain Effects | | | | | |
|------------------------|---------------------------------|----------------------------------|-----------------------------------|--------------------------------------|----------------------------------|
| Score | $p_{(ANOVA)}$ | $\mu_{(BL/6)}$ | $\mu_{(129S6)}$ | $\Delta\mu \pm SD$ | $p_{(t-test)}$ |
| FP Effacement | 0.0262* | 0.333 | 0.833 | 0.500 \pm 0.219 | 0.0325* |
| Podocyte Vacuolization | 0.0499* | N/A | N/A | N/A | N/A |
| Microvillous Change | 0.0114* | 2.08 | 1.50 | -0.583 \pm 0.212 | 0.0115* |

| Time of Exposure Effects (2- Way ANOVA) | |
|--|----------|
| Score | p |
| Cumulative Podocyte | 0.0422* |
| Cumulative GBM | 0.0212* |
| Cumulative Overall | 0.0289* |

| Time of Exposure Effects (Tukey) | | | | |
|---|-----------------------------------|---------------------------------|-------------------------------|----------|
| Score | $\mu_{(7d/1d)}$ | $\mu_{(42d)}$ | $\Delta\mu$ | p |
| Cumulative Podocyte (7 x 42 days) | 3.50 | 5.33 | 1.83 | 0.0474* |
| Cumulative GBM (1 x 42 days) | 1.67 | 3.83 | 2.17 | 0.0382* |
| Cumulative Overall (1 x 42 days) | 10.2 | 18.7 | 8.50 | 0.0193* |

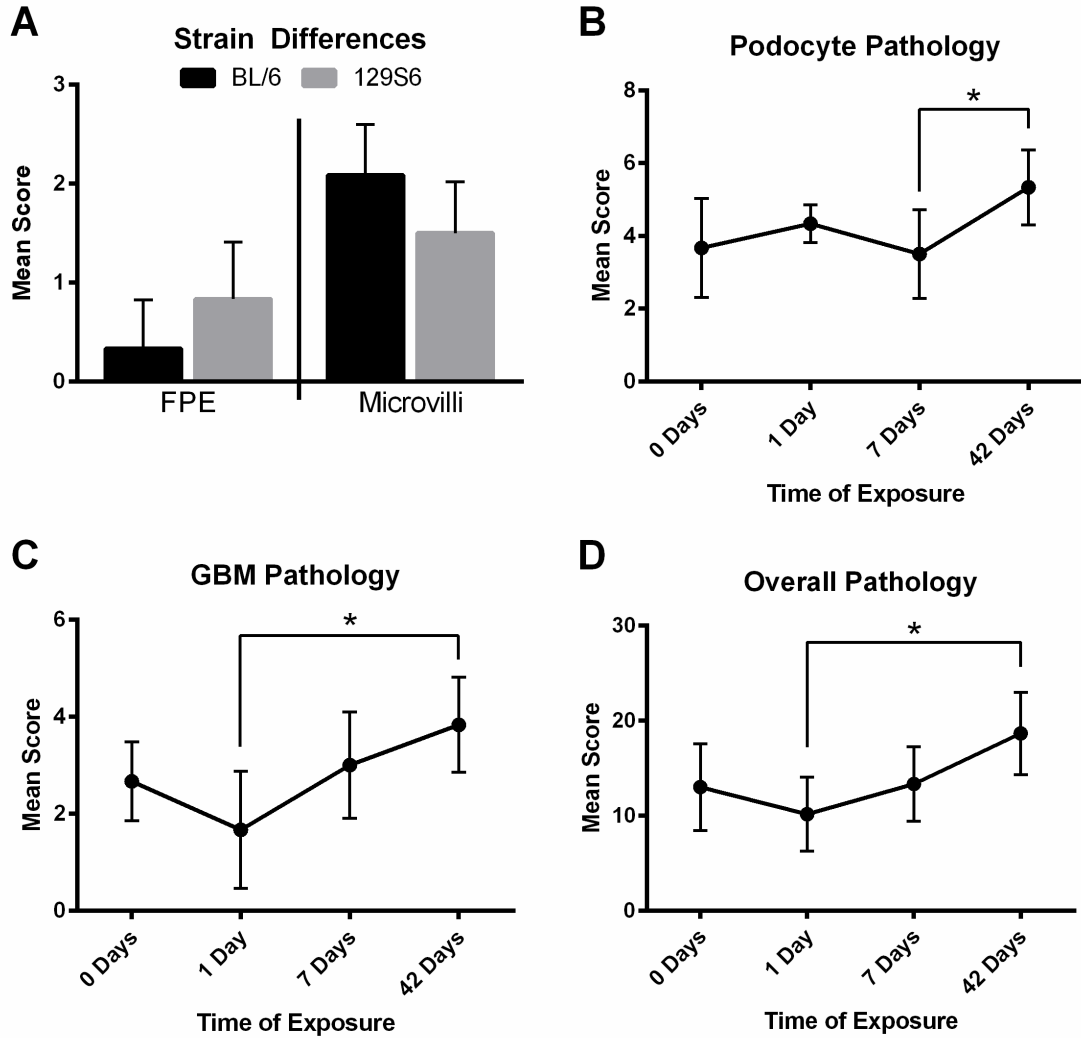


Figure 4: Mean histopathology scores in post-hoc tests. Strain differences were observed for FPE (A, left) and podocyte microvillous change (A, right), with the 129S6 strain having greater FPE scores ($p=0.0325$) and the BL/6 strain having greater microvillous change scores ($p=0.0114$) by unpaired t-test. Podocyte pathology scores were significantly greater at 42 days than those at 7 days (B, $p=0.0474$). GBM and overall pathology scores were significantly greater at 42 days than those at 1 day (C, D, $p=0.0212$ and 0.0289 , respectively). B-D derived from post-hoc Tukey multiple comparisons test. Error bars indicate standard deviation. Brackets with asterisks (*) indicate significant ($p < 0.05$) differences. All statistics performed and graphs generated using GraphPad Prism software.

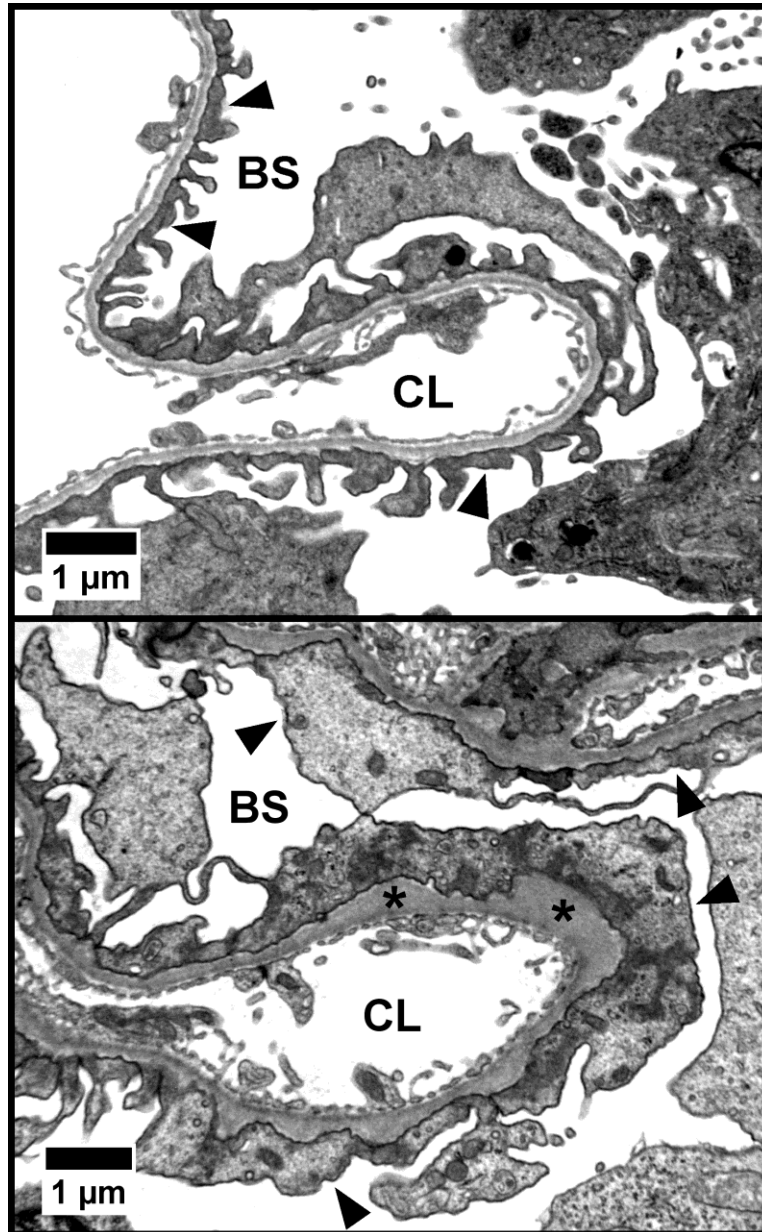


Figure 5: Representative images of foot process effacement. FPE was significantly more severe in 129S6 mice than BL/6 mice ($p < 0.04$). Pictured: Digital transmission electron micrographs of 129S6 mouse kidney in the 42-day exposure group with considerable FPE. In the top image, irregular and elongated FPs indicate early stages of podocyte injury. In the bottom image, FPs are overtly effaced. Arrowheads indicate irregular FPs in the top image and effaced FPs in the bottom image. Dense bands, likely elements of the cytoskeleton, can be observed in the effaced processes in the bottom image. The GBM in the bottom image is highly irregular with thickened regions where extra matrix lies, indicated by asterisks (*), whereas in the top image it is noticeably thin. Both images taken at 10,000X and processed using ImageJ⁴⁸. BS= Bowman's space, CL= Capillary lumen.

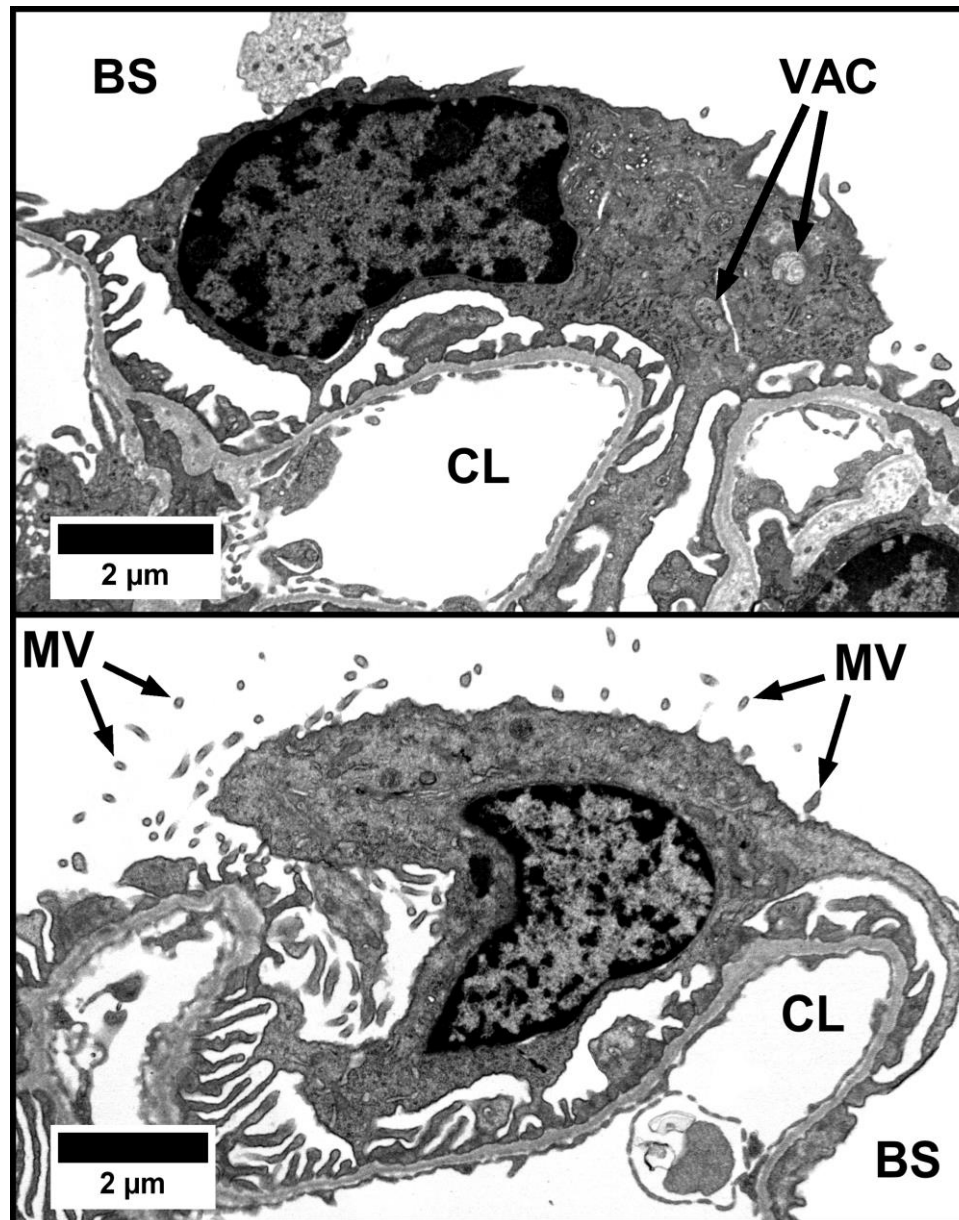


Figure 6: Representative images of podocyte vacuoles and microvillous change. Podocyte vacuolization was observed exclusively in BL/6 mice, but this observation is statistically significant ($p < 0.05$). Microvillous change was significantly more severe in BL/6 mice compared to 129S6 mice ($p < 0.02$). Pictured: Digital transmission electron micrographs of 1-day exposure BL/6 mouse kidney (top) and 42-day exposure BL/6 mouse kidney (bottom). In the top image, vacuoles are visible inside the cytoplasm of the podocyte (VAC). The podocyte in the bottom image is surrounded by multiple obliquely-sectioned microvilli (MV), presumably originating from that cell. Note also the strange debris enclosed within a loop of endothelium in the capillary lumen (CL) in the lower left quadrant. Both images taken at 10,000X magnification and processed using ImageJ⁴⁸. BS=Bowman's space.

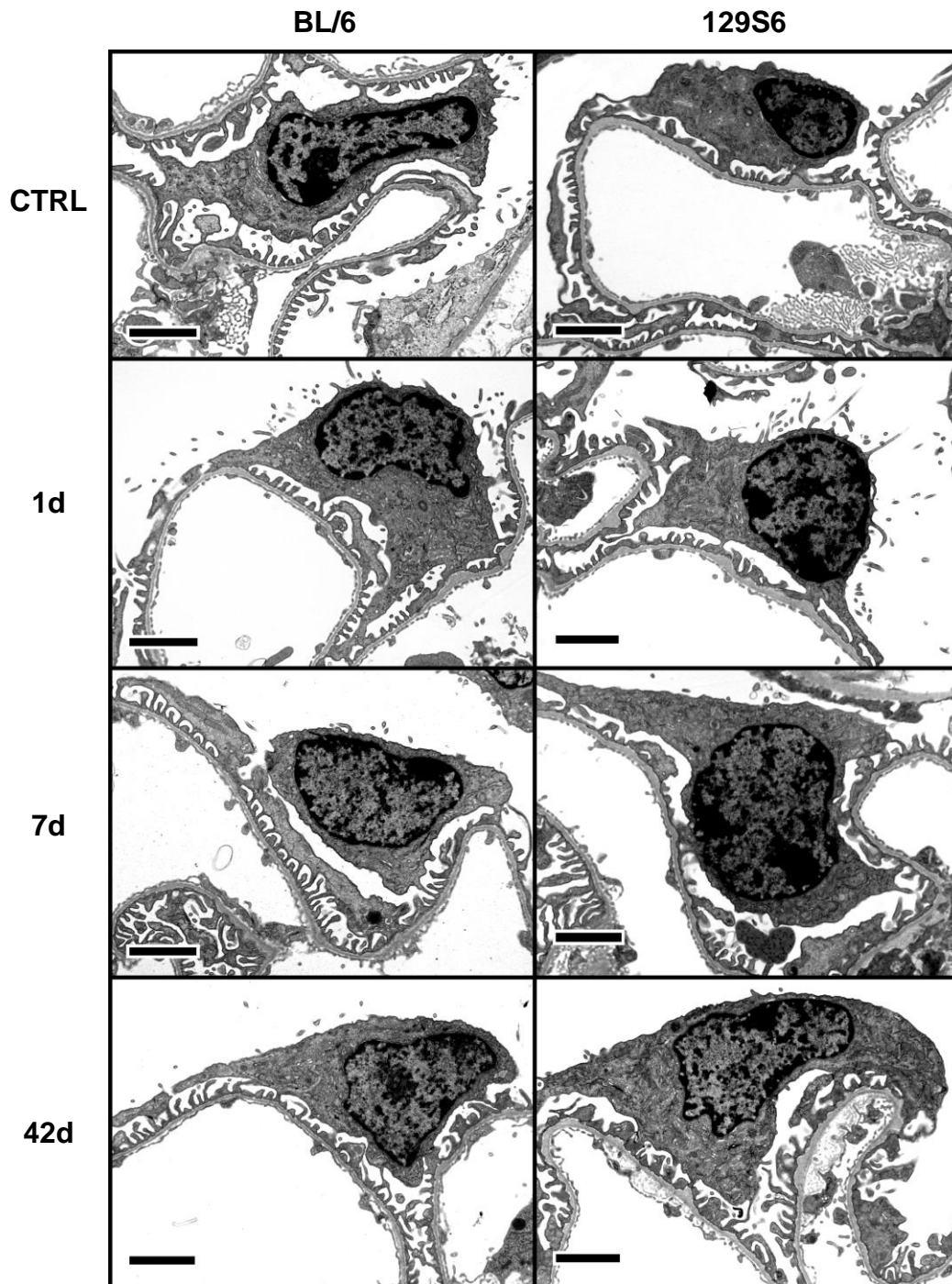


Figure 7: Representative images of capillary loops from controls and animals in all experimental groups. Pictured: Digital transmission electron micrographs, originally taken at 10,000X magnification. Images selected primarily on the basis of variables determined to be significant. Black scale bars indicate distance of 2 μ m. All images processed using ImageJ⁴⁸.

DISCUSSION

The aim of this study was to explore the pathological consequences of glomerular hypertension in the kidneys of mice with differing susceptibilities to renal injury. Towards this end, we employed a well-known model of hypertensive kidney disease in two different strains of mice and subjected them to varying lengths of exposure. The kidneys of these mice were then examined by TEM to evaluate lesions at the ultrastructural level and determine if disease or genetic predisposition has any influence on their course. Our observations show that both variables affected the pathology of these animals independently of one another and within different domains of the glomerulus.

We hypothesized that certain glomerular lesions, particularly those involving the ultrastructure of podocytes and the GBM, would be more pronounced in the injury-prone 129S6 mice. Our results demonstrate that this theory was at least partially correct. As predicted, those lesions most significantly affected by strain differences were exclusively observed within the podocyte domain. Moreover, FPE, a lesion central to the pathology of CKD and other renal disorders, was significantly more severe in the susceptible 129S6 strain than in the resistant BL/6 strain. Such a difference may explain the observations of Salzler et al. in their physiological study of 129S6 and BL/6 mice using the remnant kidney model. This group demonstrated greater overall pathology at the light microscopy level as well as albuminuria after renal ablation in 129S6 mice compared to BL/6 mice, findings consistent with more severe disease in the susceptible strain. If FPE is indeed a

consequence of glomerular injury that precipitates nephrosis and progressive disease, our evidence further implicates the role of genetic predisposition in the pathogenesis of CKD.

Unexpectedly, certain podocyte changes associated with human kidney disease were observed to a higher degree in the supposedly injury-resistant BL/6 mice. One of these lesions, the presence of pathological vacuoles in the cytoplasm of podocytes, was observed exclusively in BL/6 mice. These vacuoles are thought to contain products of autophagy reflecting increased turnover of cellular material³³ as the podocyte adapts to the changing conditions at the glomerulus or suffers damage as a result of physiological insult. Pseudocysts have been previously observed in the cell bodies of rat podocytes subjected to hypertensive injury³⁰, however we observed these structures only in the podocytes of time zero controls and 1-day exposure mice. It should be noted that we observed these vacuoles only under isolated circumstances; the highest score assigned to vacuolization was 1. Our findings suggest that vacuolization or pseudocyst formation may be a normal process of podocytes in mice, but more thorough exploration of normal murine ultrastructure is required to substantiate this claim.

BL/6 mice were also observed to have more pronounced apical microvillous formation in our study. Microvillous change is a finding thought to indicate ongoing adaptation in podocytes, as the cytoplasm of the cell reaches out in search of stable attachments to brace itself against the increasing physical and hydraulic pressures of the glomerulus²². Previous ultrastructural studies of the glomerulus have reported microvillous change in injured podocytes³³ and have associated this change with a process of glomerulosclerosis known as crescent formation, in which part of the glomerulus becomes

attached to the parietal wall of the renal corpuscle and develops into a scar²². To date, microvillous change in podocytes has not been rigorously characterized. Our findings suggest that this change may be worth more thorough investigation; however the context in which it was observed calls its role in disease into question. Microvillous change was present in nearly equal severity across all exposure groups in the BL/6 mice including time zero controls, indicating that apical microvilli may be a normal characteristic of murine podocytes. Further investigation is warranted to discern these differences.

Duration of GHT exerted significant influence on the severity of kidney pathology in both strains of mice. As hypothesized, longer periods of exposure were associated with more pronounced pathology in both the podocyte and GBM domains as well as greater overall pathology. Interestingly, length of exposure was found to be associated with increased cumulative pathology scores rather than the prevalence of specific lesions. The implications of this finding on the association between cardiovascular and kidney disease are manifold.

Although the endothelium is the only element of the glomerulus specific to the cardiovascular system, we did not observe that duration of GHT had any significant effect on its morphological pathology. Moreover, the endothelium was arguably the least affected, with cumulative endothelium scores having the least significant association with length of exposure among all domain scores ($p > 0.2$). The elements that were affected by GHT duration were those not present in the extra-renal vasculature, specifically the specialized basement membrane of the glomerulus and its opposing epithelium, the podocytes. If GHT is a putative source of injury in the pathogenesis of CKD, our findings

suggest that the renal endothelium is much better-equipped to mitigate its damaging effects than the other structures of the glomerulus.

We observed that cumulative podocyte and GBM pathology scores were significantly greater at 42 days of exposure than at 7 days or 1 day, respectively. As the remaining two elements of the filtration barrier, these observations are not unexpected given their important roles in maintaining and regulating permselectivity at the glomerulus. In fact, it is logical that these two structures are highly affected by changing hemodynamic conditions across the barrier as they represent the most structurally stabilizing and selective elements of the biological sieve.

The GBM, a sheet of collagen, laminins, and other matrix materials, is responsible for both containing the blood within the lumen of glomerular capillaries and restricting passage of large anionic molecules into Bowman's space. Hypertension subjects the GBM to considerable stretching forces, distending the capillary lumen and weakening the integrity of the membrane³². Changes in GBM thickness have been associated with FSGS in nephrotic patients¹⁹ as well as other forms of kidney disease, but the nature of this change is variable. An intuitive theory might suggest that thinning of the GBM weakens the barrier and potentiates albuminuria while thickening of the GBM reflects sclerotic changes in response to injury. Indeed, it seems plausible that increased hydraulic pressure and fluid flow could simultaneously weaken the structural integrity of the membrane and encourage filtration of normally excluded substances. We observed only thinning of the GBM, however it was the cumulative GBM score which includes irregularity (degree of

variability in thickness or composition) that was significantly affected by duration of GHT in our study.

Although mesangial expansion and deposit formation are implicated in glomerulosclerosis^{19,30}, these changes were not significantly affected by our experimental conditions. The mesangium is a dynamic structure which is responsible for maintaining the structural integrity of the glomerulus, however it does not participate in regulating permselectivity at the filtration barrier. In glomerulosclerosis the mesangium appears to replace injured capillary loops with additional matrix material, possibly to control the extravasation of important plasma protein as the GBM is denuded by podocyte loss. Our observations further suggest that GHT exerts its pathological influence primarily at the filtration barrier, making changes in the mesangium secondary to hypertensive injury.

We observed several interesting lesions during the course of our study in addition to those quantified (**Figure 8, 9**). Membrane-bound structures containing a material less dense than the cytoplasm of neighboring cells frequently appeared in the Bowman's space of both strains of mice across all time points (**Figure 8**). While the source of these structures is somewhat unclear, organelle remnants including those of mitochondria can be observed within some, indicating a cellular origin. Podocytes have been shown to shed pieces of their cytoplasm in response to injury³³, however the fact that these structures are present in the renal corpuscles of control mice discourages the idea of a pathological etiology. Additionally, podocytes were observed detaching from the basement membrane and even ejecting their cellular contents (**Figure 9**). Detached podocytes were found exclusively within the 42-day exposure group, further suggesting that denudation of the

GBM is an important element in the pathophysiology of kidney disease, albeit at a later stage.

One aim of this study was to identify early and potentially subtle ultrastructural changes that can be detected in the glomerulus after the onset of hypertension. A logical model of disease progression would suggest that ultrastructural changes precede those observable at the light microscopic level³⁴, and given the insidious nature of CKD any effort towards early detection is advantageous both for the patient and the industry as a whole. Unfortunately, we failed to detect morphological changes at early time points that differed from the control group and in fact observed a pattern of variation in which some scores appeared to be lower (i.e. less damage was seen) after short durations of exposure than those right after surgery. While this variation may be attributable to real ultrastructural dynamics in response to kidney injury, the limitations of this study must be considered before speculation is made.

Our ability to observe significant but subtle changes in the glomerular architecture was likely limited by several factors. First, the subjective nature of our study relied upon the experience of the renal pathologist to quantify the extent of lesions using a somewhat arbitrary scoring system, restricting the applicability of our data to mostly qualitative conclusions. Additionally, small sample size (n=24 scores/lesion) reduced the power of our analysis, making it more difficult to reject the null hypothesis that the effects we observed were random and not attributable to experimental conditions. Careful consideration of the data reveals that the variation observed between early time points is within experimental error and therefore insignificant in a study of this size.

The process of tissue harvest, fixation and embedding may have also introduced changes in morphology not attributable to experimental conditions. Due to the time and resources necessary for tissue processing, not all tissue was processed simultaneously and some specimens were left in initial fixative longer than others. Changes in the integrity of membranes or the osmotic qualities of the tissue caused by processing therefore may have affected their appearance by TEM. Fortunately, such changes would likely have little effect on our subjective interpretations, as processing artifacts frequently manifest as alterations in the absolute size or volume of cellular structures rather than their general appearance.

Our subjective approach aimed to improve our general understanding of the histopathology of hypertensive mice, considering the lack of ultrastructural data in murine models of kidney disease. Techniques do exist, however, to objectively quantify the properties of some lesions considered in this study^{20,45}. For example, FPE was a lesion observed to be significantly dependent upon strain in these mice. FPE has been quantified by several TEM methods, such as counting the frequency of filtration slits along a given distance of GBM and measuring the mean width of FPs at the membrane²⁰. Future studies will aim to further characterize FPE in DOCA-UNX mice through objective quantification in order to more robustly analyze the relevance of podocyte morphology in hypertensive kidney disease. We also observed a significant association between GBM pathology and duration of GHT. GBM thickness measurements are currently standard protocol in renal TEM biopsy and such a technique could be employed to quantify changes in the character of the GBM in DOCA-UNX mice.

In sum, we have performed a detailed assessment of the renal histopathology of hypertensive mice by TEM. Moreover, we have examined the effects of genetic predisposition as well as GHT in CKD pathogenesis and found that both variables exert significant effects on different aspects of glomerular pathology. We hypothesized that genetic susceptibility, represented by the 129S6 strain of mice, as well as increased duration of GHT exposure would be associated with more severe ultrastructural histopathology. Our findings suggest that this hypothesis is partially correct. Genetic susceptibility was associated with a greater degree of FPE, the cardinal sign of glomerular podocyte injury; however, supposed genetic resistance (represented by the B6 strain) was associated with a greater prevalence of other podocyte lesions. Both cytoplasmic vacuoles and apical microvilli, lesions commonly associated with human renal pathology, were observed more frequently in the purportedly CKD-resistant C57BL/6 strain of mice. GHT had a significant effect on collective podocyte, GBM, and overall pathology, with increased duration of exposure associated with greater histopathological severity. Our results provide a foundation for future studies of glomerular dynamics using the DOCA-UNX model in mice, furthering efforts to lessen the hardship of those with CKD.

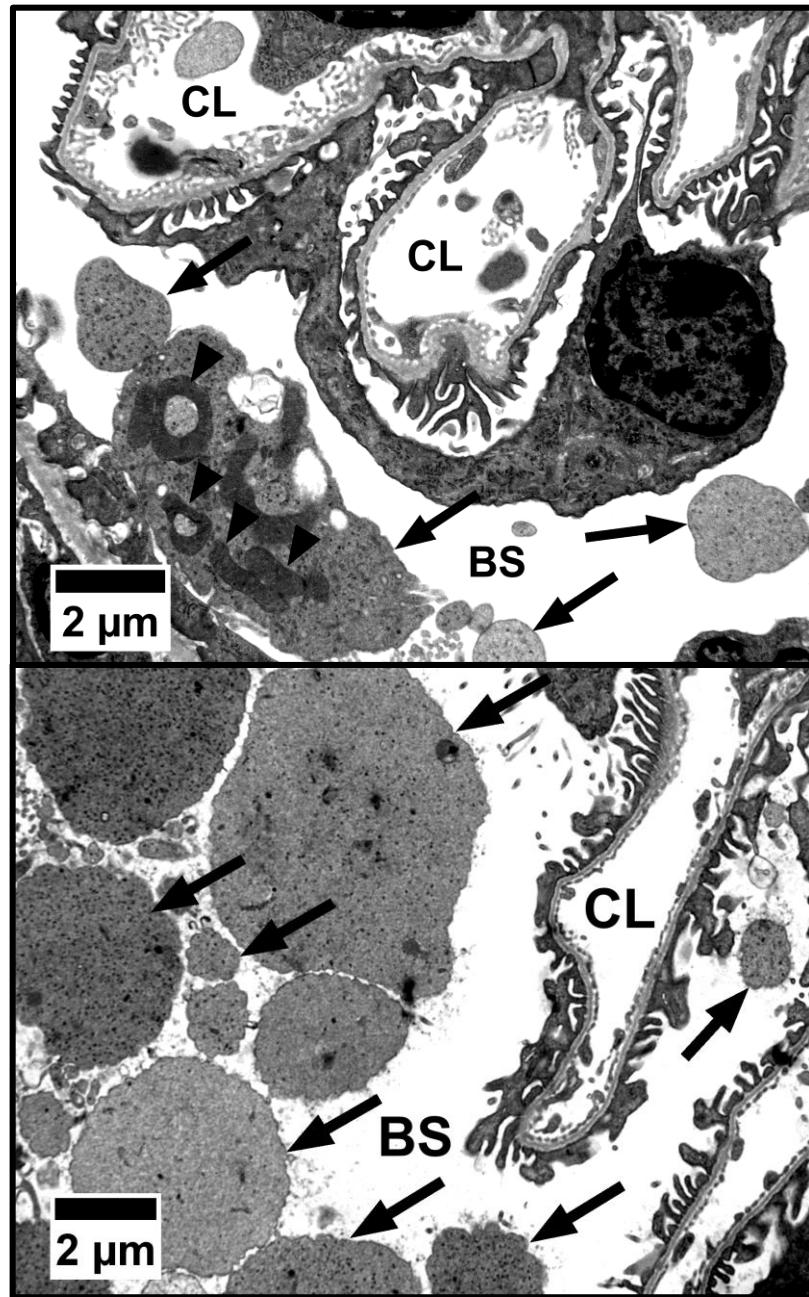


Figure 8: Membrane-bound structures in Bowman's space. Pictured: Digital transmission electron micrographs of 129S6 (top) and BL/6 (bottom) mouse kidneys, from time zero and 1-day exposure groups, respectively. Membrane-bound organelles (arrows) of unknown origin were observed in the Bowman's spaces of these mice. Organelle remnants, specifically those of mitochondria, can be seen within some of these organelles (arrowheads). Top image originally taken at 10,000X magnification, bottom image originally taken at 6,000X magnification. Tissue prepared as described in methods. Both images processed using ImageJ⁴⁸. BS= Bowman's space, CL=Capillary lumen.

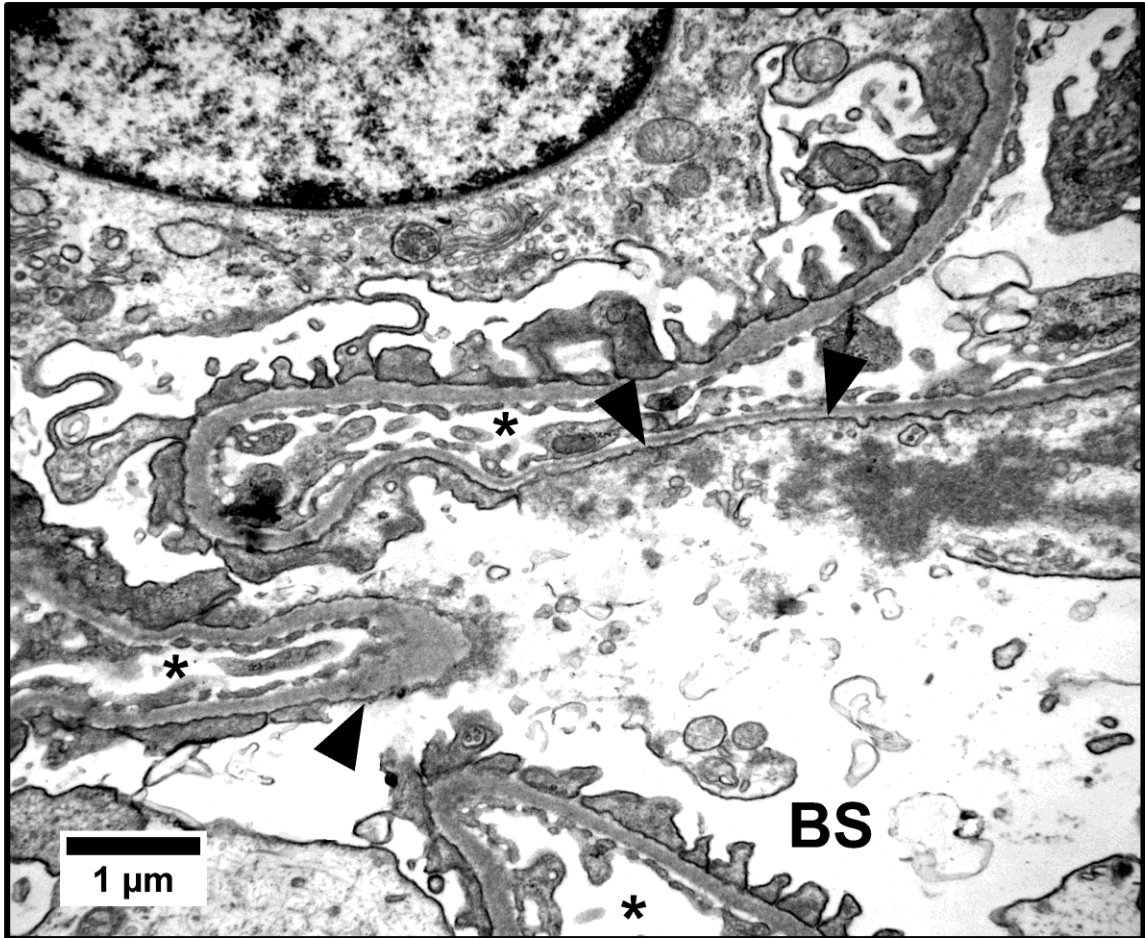


Figure 9: Epithelial lysis and denudation of the glomerular basement membrane. Podocyte detachment leaves bare segments of the GBM, compromising the filtration barrier at these segments and likely allowing the passage of plasma protein into Bowman's space (BS). Detachment is thought to be secondary to FPE and reflects critical injury of the podocyte or failure of the podocyte's attachments to the GBM. Here a podocyte appears to have lysed catastrophically, leaving segments of bare GBM (arrowheads). It should be noted that this appearance could also be due to artifact; however lysed cells were only observed in the 42-day exposure group across both strains. Cellular debris can be observed emptying into the BS. Note the capillaries in this particular field are nearly collapsed; capillary lumens are indicated here with an asterisk (*). Also of note is the remarkably decreased density of the cytoplasm within the podocyte at the top of the image, with prominent organelles likely manufacturing products to facilitate adaptive molecular and structural changes. Pictured: 129S6 mouse kidney in the 42-day exposure group, originally taken at 20,000X magnification. Tissue prepared as described in methods. Image processed using ImageJ⁴⁸.

REFERENCES

1. Abrahamson DR. Role of the podocyte (and glomerular endothelium) in building the GBM. *Seminars in Nephrology*. 2012;32(4):342-349.
2. van den Berg JG, van den Bergh Weerman MA, Assmann KJM, Weening JJ, Florquin S. Podocyte foot process effacement is not correlated with the level of proteinuria in human glomerulopathies. *Kidney International*. 2004;66(5):1901-1906.
3. Boron WF, Boulpaep EL. *Medical Physiology: A Cellular and Molecular Approach*. Updated second edition. Philadelphia, PA: Saunders Elsevier; 2012.
4. Brenner BM, Hostetter TH, Humes HD. Molecular basis of proteinuria of glomerular origin. *New England Journal of Medicine*. 1978;298(15):826-833.
5. Brosius FC, Alpers CE, Bottinger EP, et al. Mouse models of diabetic neuropathy. *Journal of the American Society of Nephrology*. 2009;20(12):2503-2512.
6. Bruce MA, Beech BM, Crook ED, et al. Association of socioeconomic status and CKD among African Americans: The Jackson Heart Study. *American Journal of Kidney Diseases*. 2010;55(6):1001-1008.
7. Centers for Disease Control and Prevention. Chronic Kidney Disease (CKD) Surveillance System- United States. <https://nccd.cdc.gov/CKD/Default.aspx>. Published 2016. Accessed January 11, 2016.
8. Centers for Disease Control and Prevention. Prevalence of chronic kidney disease and associated risk factors -- United States, 1999-2004. *MMWR: Morbidity & Mortality Weekly Report*. 2007;56(8):161-165 5p.
9. D'Agati VD, Kaskel FJ, Falk RJ. Focal segmental glomerulosclerosis. *New England Journal of Medicine*. 2011;365(25):2398-2411.
10. Deegens JKJ, Dijkman HBPM, Borm GF, et al. Podocyte foot process effacement as a diagnostic tool in focal segmental glomerulosclerosis. *Kidney International*. 2008;74(12):1568-1576.
11. Diamond JR, Karnovsky MJ. Focal and segmental glomerulosclerosis: Analogies to atherosclerosis. *Kidney International*. 1988;33(5):917-924.
12. Dworkin LD, Hostetter TH, Rennke HG, Brenner BM. Hemodynamic basis for glomerular injury in rats with desoxycorticosterone-salt hypertension. *Journal of Clinical Investigation*. 1984;73(5):1448-1461.

13. El-Aouni C, Herbach N, Blattner SM, et al. Podocyte-specific deletion of integrin-linked kinase results in severe glomerular basement membrane alterations and progressive glomerulosclerosis. *Journal of the American Society of Nephrology*. 2006;17(5):1334-1344.
14. Endlich N, Endlich K. The challenge and response of podocytes to glomerular hypertension. *Seminars in Nephrology*. 2012;32(4):327-341.
15. Farquhar MG, Vernier RL, Good RA. An electron microscope study of the glomerulus in nephrosis, glomerulonephritis, and lupus erythematosus. *The Journal of Experimental Medicine*. 1957;106(5):649-660.
16. Flessner MF, Wyatt SB, Akylbekova EL, et al. Prevalence and awareness of CKD among African Americans: The Jackson Heart Study. *American Journal of Kidney Diseases*. 2009;53(2):238-247.
17. Friedman DJ, Pollak MR. Apolipoprotein L1 and kidney disease in African Americans. *Trends in Endocrinology & Metabolism*. 2016:204-215.
18. Genovese G, Friedman DJ, Ross MD, et al. Association of trypanolytic ApoL1 variants with kidney disease in African Americans. *Science*. 2010;329(5993):841-845.
19. Grishman E, Churg J. Focal glomerular sclerosis in nephrotic patients: An electron microscopic study of glomerular podocytes. *Kidney International*. 1975;7:111-122.
20. Gundersen HJG, Seefeldt T, Østerby R. Glomerular epithelial foot processes in normal man and rats. *Cell and Tissue Research*. 1980;205(1):147-155.
21. Herget-Rosenthal S, Dehnen D, Kribben A, Quellmann T. Progressive chronic kidney disease in primary care: Modifiable risk factors and predictive model. *Preventive Medicine*. 2013;57(4):357-362.
22. Hir ML, Keller C, Eschmann V, Hähnel B, Hosser H, Kriz W. Podocyte bridges between the tuft and Bowman's capsule: An early event in experimental crescentic glomerulonephritis. *Journal of the American Society of Nephrology*. 2001;12(10):2060-2071.
23. James MT, Hemmelgarn BR, Tonelli M. Early recognition and prevention of chronic kidney disease. *The Lancet*. 2010;375(9722):1296-1309.
24. Johnson RJ. What mediates progressive glomerulosclerosis? The glomerular endothelium comes of age. *American Journal of Pathology*. 1997;151(5):1179-1181.

25. Kanwar YS, Linker A, Farquhar MG. Increased permeability of the glomerular basement membrane to ferritin after removal of glycosaminoglycans (heparan sulfate) by enzyme digestion. *Journal of Cell Biology*. 1980;86:688-698.
26. Kazley AS, Johnson E, Simpson K, Chavin K, Baliga P. African American patient knowledge of kidney disease: A qualitative study of those with advanced chronic kidney disease. *Chronic Illness*. 2015;11(4):245-255.
27. Kerjaschki D. Caught flat-footed: podocyte damage and the molecular bases of focal glomerulosclerosis. *Journal of Clinical Investigation*. 2001;108(11):1583-1587.
28. Kiberd BA, Clase CM. Cumulative risk for developing end-stage renal disease in the US population. *Journal of the American Society of Nephrology*. 2002;13(6):1635-1644.
29. Klag MJ, Whelton PK, Randall BL, Neaton JD, Brancati FL, Stamler J. End-stage renal disease in african-american and white men: 16-year MRFIT findings. *Journal of the American Medical Association*. 1997;277(16):1293-1298.
30. Kretzler M, Koeppen-Hagemann I, Kriz W. Podocyte damage is a critical step in the development of glomerulosclerosis in the uninephrectomised-desoxycorticosterone hypertensive rat. *Virchows Archiv*. 1994;425(2):181-193.
31. Kriz W, Kretzler M, Nagata M, et al. A frequent pathway to glomerulosclerosis: Deterioration of tuft architecture-podocyte damage-segmental sclerosis. *Kidney and Blood Pressure Research*. 1996;19(5):245-253.
32. Kriz W, Lemley KV. A potential role for mechanical forces in the detachment of podocytes and the progression of CKD. *Journal of the American Society of Nephrology*. 2015;26(2):258-269.
33. Kriz W, Shirato I, Nagata M, LeHir M, Lemley KV. The podocyte's response to stress: the enigma of foot process effacement. *American Journal of Physiology - Renal Physiology*. 2013;304(4):F333-F347.
34. Kumar V, Abbas AK, Aster JC. *Robbins Basic Pathology*. 9th ed. Philadelphia, PA: Elsevier Saunders; 2012.
35. Lees GE, Cianciolo RE, Clubb Jr. FJ. Renal biopsy and pathologic evaluation of glomerular disease. *Topics in Companion Animal Medicine*. 2011;26(3):143-153.
36. Levey AS. Measurement of renal function in chronic renal disease. *Kidney International*. 1990;38(1):167-184.

37. Levey AS, Bosch JP, Lewis JB, Green T, Rogers N, Roth D. A more accurate method to estimate glomerular filtration rate from serum creatinine: A new prediction equation. *Annals of internal medicine*. 1999;130:461-470.
38. Levey AS, Coresh J. Chronic kidney disease. *The Lancet*. 2012;379(9811):165-180.
39. Levey AS, de Jong PE, Coresh J, et al. The definition, classification, and prognosis of chronic kidney disease: a KDIGO Controversies Conference report. *Kidney International*. 2011;80(1):17-28.
40. Levey AS, Stevens LA, Coresh J. Conceptual model of CKD: Applications and implications. *American Journal of Kidney Diseases*. 2009;53(3, Supplement 3):S4-S16.
41. Levey AS, Stevens LA, Schmid CH, et al. A new equation to estimate glomerular filtration rate. *Annals of internal medicine*. 2009;150(9):604-612.
42. Menon MC, Chuang PY, He CJ, Menon MC, Chuang PY, He CJ. The glomerular filtration barrier: Components and crosstalk. *International Journal of Nephrology*. 2012;2012:e749010.
43. National Kidney Foundation. K/DOQI clinical practice guidelines for chronic kidney disease: evaluation, classification, and stratification. *American Journal of Kidney Diseases*. 2002;39(2 Suppl 1):S1-S266.
44. O'Seaghdha CM, Lyass A, Massaro JM, et al. A risk score for chronic kidney disease in the general population. *The American Journal of Medicine*. 2012;125(3):270-277.
45. Ramage IJ, Howatson AG, Mccoll JH, et al. Glomerular basement membrane thickness in children: A stereologic assessment. *Kidney International*. 2002;62(3):895-900.
46. Rennke HG, Cotran RS, Venkatachalam MA. Role of molecular charge in glomerular permeability. *Journal of Cell Biology*. 1975;67:638-646.
47. Salzler HR, Griffiths R, Ruiz P, et al. Hypertension and albuminuria in chronic kidney disease mapped to a mouse chromosome 11 locus. *Kidney International*. 2007;72(10):1226-1232.
48. Schneider CA, Rasband WS, Eliceiri KW. NIH Image to ImageJ: 25 years of image analysis. *Nature Methods*. 2012;9(7):671-675.
49. Shankland SJ. The podocyte's response to injury: Role in proteinuria and glomerulosclerosis. *Kidney International*. 2006;69(12):2131-2147.

50. Spargo BH. Practical use of electron microscopy for the diagnosis of glomerular disease. *Human Pathology*. 1975;6(4):405-420.
51. St. John PL, Abrahamson DR. Glomerular endothelial cells and podocytes jointly synthesize laminin-1 and -11 chains. *Kidney International*. 2001;60(3):1037-1046.
52. Taal MW, Brenner BM. Renal risk scores: Progress and prospects. *Kidney International*. 2008;73(11):1216-1219.
53. Tarver-Carr ME, Powe NR, Eberhardt MS, et al. Excess risk of chronic kidney disease among African-American versus white subjects in the United States: A population-based study of potential explanatory factors. *Journal of the American Society of Nephrology*. 2002;13(9):2363-2370.
54. Tzur S, Rosset S, Shemer R, et al. Missense mutations in the APOL1 gene are highly associated with end stage kidney disease risk previously attributed to the MYH9 gene. *Human Genetics*. 2010;128(3):345-350.
55. United States Renal Data System. *2015 USRDS Annual Report: Epidemiology of Kidney Disease in the United States*. Bethesda, MD: National Institutes of Health, National Institute of Diabetes and Digestive and Kidney Diseases; 2015. <http://www.usrds.org/2015/view/Default.aspx>. Accessed January 12, 2016.
56. Vart P, Gansevoort RT, Joosten MM, Bültmann U, Reijneveld SA. Socioeconomic disparities in chronic kidney disease: A systematic review and meta-analysis. *American Journal of Preventive Medicine*. 2015;48(5):580-592.
57. Vogelmann SU, Nelson WJ, Myers BD, Lemley KV. Urinary excretion of viable podocytes in health and renal disease. *American Journal of Physiology - Renal Physiology*. 2003;285(1):F40-F48.
58. Yu D, Petermann A, Kunter U, Rong S, Shankland SJ, Floege J. Urinary podocyte loss is a more specific marker of ongoing glomerular damage than proteinuria. *Journal of the American Society of Nephrology*. 2005;16(6):1733-1741.

CURRICULUM VITAE

JAMES WARE STEVENSON

(1992)

(508) 733-6003 • jsteven4@outlook.com
38 Richard Rd., Marlborough, MA 01752

EDUCATION

2016 **M.S., Medical Sciences (anticipated)**
Boston University School of Medicine
Division of Graduate Medical Sciences
Boston, MA 02118

Thesis: A morphological analysis of ultrastructural dynamics in the murine glomerulus following surgically-induced renal hypertension

2014 **B.S., Biology**
Providence College
Providence, RI 02918

PUBLICATIONS & PRESENTATIONS

2016 **Stevenson JW**, Conaty EA, Walsh RB, Poidomani PJ, Samoriski CM, Scollins BJ, & DeGiorgis JA. The amyloid precursor protein of Alzheimer's disease clusters at the organelle/microtubule interface on organelles that bind microtubules in an ATP-dependent manner. *PLoS ONE*. 2016;11(1):e0147808.

2013 **Stevenson JW** & Chichester CO. Developing inter-professional communication skills using a high-fidelity human patient simulator. Poster presentation at the International Meeting on Simulation in Healthcare, January 2013.

RESEARCH

**2015-
Present** **Investigation of the pathogenesis and pathophysiology of human chronic kidney disease.**

Primary investigator: Dr. Joel Henderson, M.D., Ph.D.

Boston University School of Medicine
Department of Pathology & Laboratory Medicine
Boston, MA 02118

2013-2014 Characterization of the amyloid precursor protein of Alzheimer's disease.

Primary investigator: Dr. Joseph DeGiorgis, Ph.D.
Providence College, Providence, RI 02918
Marine Biological Laboratory, Woods Hole, MA 02543

2012-2013 Design and development of a training exercise in inter-professional communication using high-fidelity human patient simulation.

Primary investigator: Dr. Clinton Chichester III, Ph.D.
University of Rhode Island College of Pharmacy
Kingston, RI 02881